Superpixel Generation for SAR Imagery Based on Fast DBSCAN Clustering With Edge Penalty

Liang Zhang, Shengtao Lu, Canbin Hu, Deliang Xiang, *Member, IEEE*, Tao Liu, and Yi Su, *Senior Member, IEEE*

***Abstract*—In this article, we propose an adaptive superpixel generation algorithm for synthetic aperture radar (SAR) imagery, which is implemented based on fast density-based spatial clustering of applications with noise (DBSCAN) clustering and superpixel merging with edge penalty. The superpixel generation algorithm consists of two stages, i.e., fast pixel clustering and superpixel merging. In the clustering stage, we define a new adaptive pixel dissimilarity measure for SAR image and then optimize the DBSCAN strategy, which considers the edge information and can achieve rapid clustering. In the merging stage, based on the initial superpixels, a new superpixel dissimilarity measure is defined, which can merge the small local superpixels into their neighborhood superpixels, making the final superpixel segmentation results compact and regular. Experimental results on two simulated and two real SAR images demonstrate that our method outperforms the state-of-the-art superpixel generation methods in terms of both efficiency and accuracy. The superpixel segmentation accuracy of our method is 5–10% higher and the time cost is 10–40% lower than other methods. Since the superpixel segmentation result can be used as a preprocessing stage for the SAR data interpretation applications, superpixel-based and pixel-based classification results with two real SAR images are also used for comparison, which can validate the advantages of our proposed method.**

***Index Terms*—Clustering, density-based spatial clustering of applications with noise (DBSCAN), edge penalty, superpixel generation, synthetic aperture radar (SAR) image.**

I. Introduction

In RECENT years, superpixel-based methods have attracted increasing attention for synthetic aperture radar (SAR) image interpretation for the reason that superpixels can better capture the local image information than pixels, as well as reduce the computational complexity of subsequent SAR image processing tasks. Moreover, the superpixels are beneficial to the speckle noise and artifact reduction for the SAR data. These various image degradation factors have a negative influence on remote sensing data interpretation [1]. The superpixel is a group of pixels with similar attributes, which can be regarded as a processing unit instead of pixels. The number of superpixels is much smaller than the pixel number. Thus, the superpixel-based processing methods would be more efficient than the pixel-based methods for SAR images, especially for the large image scene. More importantly, the superpixels can well adhere to the image boundaries, which can preserve the image details. Till now, superpixels have been used for various SAR image applications such as target detection [2], [3], segmentation [4] and classification [5], etc.

Until now, most of the superpixel generation methods are proposed for natural color images, such as the normalized cut [6], turbopixels [7], simple linear iterative clustering (SLIC) [8], linear spectral clustering (LSC) [9] and so on. Nevertheless, these methods cannot be directly applied to SAR images for the reason that the Euclidean distance used in these methods is not suitable for SAR images due to the speckle noise. In addition, the high dynamic range, layover, and sidelobe make the SAR image scene quite complex, resulting in poor superpixel generation performance using the aforementioned methods. To achieve the superpixel generation for SAR images, several methods have been proposed. Arisoy *et al.* [10] presented a mixture-based superpixel generation method for SAR image, which takes the amplitudes and pixel coordinates as features to finite mixture models to cluster the pixels into superpixels. Jing *et al.* [11] proposed an edge-aware (EA) superpixel generation for SAR image by taking into consideration of the edge information. Akyilmaz *et al.* [12] proposed a pixel similarity ratio (PSR) for SAR images and then used it to label the pixels within the search areas for generating superpixels on the basis of SLIC. Hu *et al.* [13] proposed a superpixel generation for SAR imagery using an edge-dominated (ED) local clustering, which is designed on the basis of the SLIC approach. Zhang *et al.* [14] proposed a fast multiscale superpixel segmentation method based on the minimum spanning tree. Ghaffari *et al.* [15] proposed a weighted conditional random fields algorithm based on a two-step superpixel generation method for SAR images where the intensity heterogeneity due to speckle and backscattering is considered for the superpixel segmentation. Wang *et al.* [16] developed a superpixel segmentation approach and extended its application on ship target detection for marine SAR images, which incorporated a Fisher vector (FV) to improve low contrast between the ship targets and sea clutter, increasing the discrimination accuracy. Shang *et al.* [17] proposed to use the SLIC algorithm

Manuscript received October 14, 2021; revised November 18, 2021; accepted November 24, 2021. Date of publication November 30, 2021; date of current version January 12, 2022. This work was supported by the National Natural Science Foundation of China under Grant 41801236, Grant 61901501, and Grant 62171015. *(Corresponding author: Deliang Xiang.)*

Liang Zhang, Tao Liu, and Yi Su are with the College of Electronic Science, National University of Defense Technology, Changsha 410073, China (e-mail: zl110119@163.com; liutao.apo@gmail.com; y.su@yeah.net).

Shengtao Lu and Canbin Hu are with the College of Information Science and Technology, Beijing University of Chemical Technology, Beijing 100029, China (e-mail: lst971118@163.com; canbinhu@163.com).

Deliang Xiang is with the Beijing Advanced Innovation Center for Soft Matter Science and Engineering, Beijing 100029, China, and also with the Interdisciplinary Research Center for Artificial Intelligence, Beijing University of Chemical Technology, Beijing 100029, China (e-mail: xiangdeliang@gmail.com).

Digital Object Identifier 10.1109/JSTARS.2021.3131187

to generate superpixels, and then used strong SAR image edges as constraints to calculate the neighborhood weighted mean of each superpixel to achieve the superpixel smoothing.

In recent years, there have been proposed some superpixel generation methods based on deep learning models. Yang *et al.* [18] incorporated the superpixel generation into deep neural networks to achieve image segmentation. Lv *et al.* [19] extracted the temporal change feature from superpixel with noise suppression and then incorporated them with the auto contractive autoencoder. In addition to the superpixel generation methods, there are some superpixel-based or region-based classification applications, such as the remote sensing imagery classification [20]–[22], change detection [23], image denoising [24], etc.

Apart from the above superpixel generation methods for single-polarization SAR images, there are also some superpixel generation methods for fully polarimetric SAR images. Based on the SLIC framework, Feng *et al.* [25], Song *et al.* [26], and Qin *et al.* [5] proposed to use the symmetric revised Wishart distance, Bartlett distance, and revised Wishart distance, respectively, to replace the Euclidean distance in the original SLIC produce for PolSAR image superpixel generation. Xiang *et al.* [4] proposed an adaptive superpixel generation method for PolSAR images, which can automatically control the balance between superpixel shape and compactness. Wang *et al.* [6] tried to use the entropy rate superpixel method in PolSAR image superpixel generation. Liu *et al.* [2] introduced the normalized cuts approach into the superpixel generation of PolSAR images based on the edge maps. Lang *et al.* [27] proposed a generalized mean shift algorithm and then extended it for PolSAR superpixel segmentation, which can achieve fine segmentation results for PolSAR data. Yin *et al.* [28] modified the SLIC clustering function to adapt the characteristics of polarimetric statistical measures and then proposed a superpixel segmentation method for PolSAR images.

Although the above methods can achieve superpixel generation for SAR and PolSAR images, there are some deficiencies. On the one hand, some methods such as [10], [12] are designed on the basis of SLIC algorithm. The main shortcoming is that they only use the image intensity and location information as features without considering the edge information to define the dissimilarity measure, resulting in that the superpixels cannot well adhere to the true object boundaries. Although the edge information of SAR imagery is considered in some methods [11], [13], they are not fully used for the dissimilarity measure. The edge strength result is regarded as a guidance map for the superpixel generation. In addition, the generated superpixels cannot be well adaptive to the complex SAR image scene [14]. For instance, superpixels within homogeneous areas should be regular and compact whereas in heterogeneous areas, they tend to have different shapes to well adhere to the complex image object boundaries. On the other hand, the method like [10] has a high computational cost as a preprocessing method due to the model parameter estimation. Therefore, it is necessary to conduct an adaptive and fast superpixel generation method for SAR image, which can be adaptive to the complex SAR image scene.

To achieve the above expectation, we propose an adaptive superpixel generation algorithm for SAR image based on the density-based spatial clustering of applications with noise (DBSCAN) strategy, which is implemented based on fast clustering and superpixel merging with edge penalty. In comparison with other state-of-the-art methods, our proposed method has the following contributions and advantages.

1) The edge strength map is obtained from SAR imagery by using our previously proposed edge detector [29], which is then considered in the definitions of pixel and superpixel dissimilarity measure and DBSCAN optimization. Thus, the proposed method can incorporate the edge information into the superpixel generation, resulting in satisfactory superpixels with good boundary adherence.
2) The local homogeneity measurement of SAR images is taken into consideration for the definition of dissimilarity measure, making the proposed superpixel generation adaptive to the complex SAR image scene. Therefore, the superpixels in homogeneous and heterogeneous areas would change the shapes and compactness accordingly, leading to a better preservation ability of SAR image details.
3) Apart from the pixel dissimilarity, we also define a new superpixel dissimilarity measure, which can merge the small local superpixels into their neighborhood superpixels, making the final superpixel segmentation results compact and regular. Therefore, there are few over-segmentation errors in the result of our method.

The rest of this article is organized as follows. Section II gives the background and some related works of the proposed method. Section III shows the detailed descriptions of the proposed method, which consists of edge extraction, initial superpixel generation, and superpixel merging. In Section IV, we provide in-depth comparisons between the proposed algorithm and other existing algorithms via detailed experiments using simulated and real SAR datasets. The superpixel generation results of different methods, as well as the superpixel-based applications, are compared. In addition, the computational complexity analysis and time costs are also given. Section V concludes this article with some remarks and directions for plausible future research.

II. Background and Related Works

As we stated in the introduction section, superpixel generation is popular and widely used in natural images, however, they cannot be directly used for SAR images for the reason that SAR images suffer from multiplicative speckle noise, relatively high dynamic range, layover, and sidelobe, making the SAR image scene quite complex. For one SAR image I, the multiplicative speckle model can be generally depicted as

$$I = \Omega_R \cdot N_S \tag{1}$$

where I is the original SAR image intensity, Ω_R is the backscattering coefficient of the pixels, and N_S is the speckle noise within the SAR image, which is considered to obey a Gamma distribution with unit mean [30].

The superpixel generation algorithm called SLIC [8] has been widely used for natural images and performs satisfactorily in

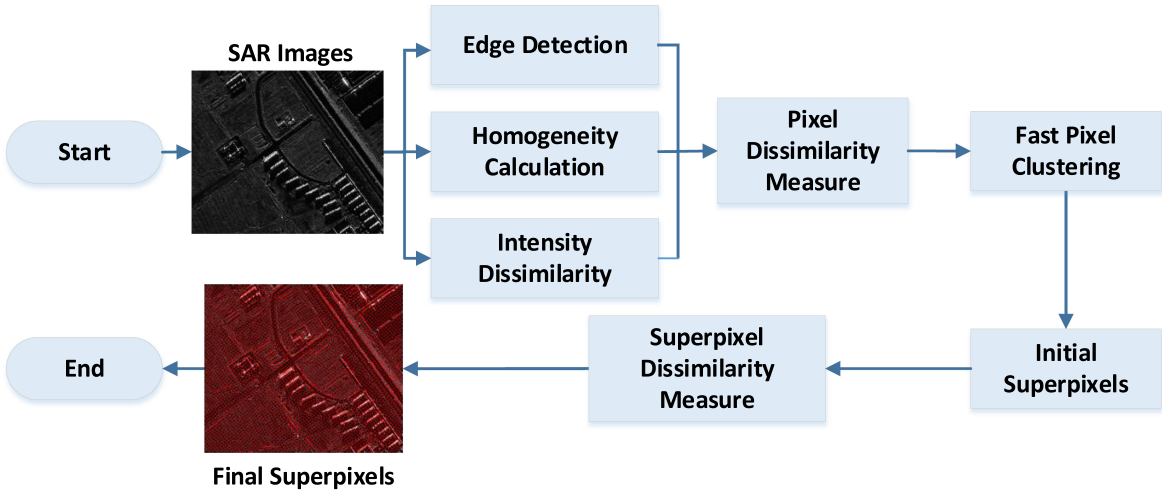

Fig. 1. Flowchart of the proposed superpixel generation algorithm.

terms of both boundary adherence and efficiency. Let S and K be the image size and the number of superpixels, respectively. The main stages of the standard SLIC method are depicted as follows:

1) Initialization of the cluster centers. Set K initial cluster centers on a regular grid, and then move these cluster centers to the positions with the lowest gradients in a 3×3 neighborhood;
2) Pixels local clustering. Assign each pixel to the closest cluster center in a local search area by the k-means clustering;
3) Update cluster centers. The cluster center is updated as the mean of all pixels which belong to it;
4) Repeat the steps 2) and 3) until the termination condition is achieved; and
5) Post-processing. The isolated regions are reassigned to neighbor superpixels if the size of the isolated regions is smaller than a threshold.

In the standard SLIC approach, the Euclidean distance is used in the local k-means clustering, which is not suitable for the SAR images with multiplicative noise [5], [31]. Although there are some variants of the SLIC approach for SAR image superpixel generation, there are some drawbacks. The edge information of the SAR images is not fully considered. Moreover, the superpixel generation cannot be adaptive to the complex SAR image content.

Not that the density-based clustering methods have the advantages that they can find arbitrary shaped clusters in the dataset and also insensitive to noise. In these methods, the clusters are formed by merging dense areas separated by spares areas. DBSCAN is one of the density-based clustering methods and proposed for clustering large spatial databases with noise or outliers. However, it is seldom used for superpixel generation. Therefore, in this work, we adopt the DBSCAN clustering method for SAR image superpixel generation, which also tries to resolve the drawbacks that the superpixel generation is not robust to the multiplicative speckle noise and is not adaptive to the complex SAR image scene.

III. Proposed Methodology

In this section, we introduce the main components of our proposed superpixel generation algorithm. It consists of two stages, i.e., fast pixel clustering and superpixel merging, which is designed based on the proposed pixel dissimilarity measure and superpixel dissimilarity measure. The DBSCAN strategy is optimized with the edge information which is extracted from the SAR images. The flowchart of our proposed algorithm is shown in Fig. 1 and the individual components are given in detail in different subsections, as well as the implementations of the algorithms.

A. Edge Information Extraction From SAR Image

There have been proposed several edge detection methods for SAR images [32]–[34]. In this article, we adopt our previously proposed edge detector with a recurrent guidance filter to extract edge information from SAR images [29]. In this method, the recurrent guidance filter contains two stages, where the first stage is to use the Gaussian filter to remove texture and speckle, increasing the edge information. After that, the filtered SAR image is used for edge extraction to preserve the edges in an iterative manner.

First, the Gaussian filter is used to suppress the texture information and speckle within the SAR images, making the edges be well preserved. This stage is beneficial to the SAR edge extraction for the reason that the edges can be relatively enhanced. After that, in the next iteration, the obtained Gaussian-filtered image can be regarded as the new guidance image to filter the input SAR image, resulting in that the guidance image being iteratively updated. Therefore, when the iteration terminates, we can obtain the final filtered image. It can be seen that this stage is an iteration manner and the filter can be called a recurrent guidance filter.

The recurrent guidance filter for each pixel in the SAR image is given as [29]

$$J^t(p) = \frac{1}{K_p} \sum_{q \in N(p)} \exp\left(-\frac{\|p-q\|^2}{2\sigma_s^2}\right) \times \exp\left(-\frac{GLR_{J^{t-1}}(p,q)}{2\sigma_r^2}\right) I(q) \quad (2)$$

where $J^t(p)$ represents the filtered result of the pixel p in the tth iteration. $I(q)$ is the intensity of pixel q in the SAR image I. The spatial and intensity weights are controlled by σ_s and σ_r. $N(p)$ is the set of neighboring pixels surrounding the pixel p. $GLR_{J^{t-1}}(p,q)$ indicates the dissimilarity between p and q in the guidance image J^{t-1}, which can be defined as [29]

$$GLR_{J^{t-1}}(p,q) = 2 \cdot M \cdot \ln \frac{\bar{J}^{t-1}(p) + \bar{J}^{t-1}(q)}{2\sqrt{\bar{J}^{t-1}(p) \cdot \bar{J}^{t-1}(q)}} \quad (3)$$

where M indicates the neighboring pixel number for each center pixel. The K_p in (2) is defined as

$$K_p = \sum_{q \in N(p)} \exp\left(-\frac{\|p-q\|^2}{2\sigma_s^2}\right) \cdot \exp\left(-\frac{GLR(p,q)}{2\sigma_r^2}\right) \quad (4)$$

which is used for normalization. The recurrent guidance filter in (2) is constructed on a joint bilateral filter and employed iteratively, aiming to remove the nonedge information including speckle and texture and preserve the edge information. Then the edge detector with the Gaussian-shaped window is adopted to extract the final edge strength map. The algorithm can be implemented according to Algorithm 1. Further details can be found in [29].

It is worth pointing out that in Algorithm 1, there are several parameters that can influence the edge detection performance. The parameters σ_s and σ_r can be set as 3 and 0.03, respectively. It should be noted that these two parameters are not sensitive to the SAR imagery. Therefore, it can be set the fixed values. Th_{low} and Th_{high} are used to determine the edge pixels from the edge strength map, which can be set as 0.08 and 0.14, respectively. They can be adjusted accordingly if necessary when dealing with SAR images.

Fig. 2 gives the edge detection performance of the utilized detector, where Fig. 2(a) is the original SAR image and Fig. 2(b) is the edge strength map of the detector. Fig. 2(c) and (d) is the edge map of the Gaussian-shaped window edge detector without and with the recurrent guidance filter. It can be seen that by using the recurrent guidance filter, the speckle noise can be suppressed and the isolated pixels can be eliminated in the final edge map, which can increase the edge detection accuracy.

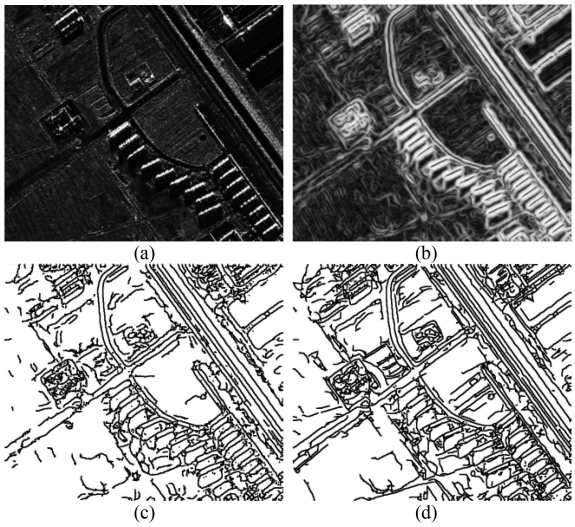

Fig. 2. Edge detection performance of the utilized detector. (a) Original SAR image. (b) Edge strength map of the detector. (c) Edge map of Gaussian-shaped window edge detector without considering the recurrent guidance filter. (d) Edge map of the Gaussian-shaped window edge detector considering the recurrent guidance filter.

B. Initial Superpixel Generation With Fast Clustering Stage

First of all, we aggregate pixels to get initial superpixels with the fast clustering stage. DBSCAN is the pioneer of density-based clustering techniques that can discover clusters of arbitrary shape and also handle noise or outliers [35], [36]. Given a set of feature points, DBSCAN can group the points that are closely packed together (i.e., the points with many nearby neighbors). In contrast, the outlier points stay alone in low-density regions whose nearest neighbors are too far away from them. Moreover, it can be extended to large datasets by reducing its time complexity using spatial index structures. DBSCAN is one of the most common local clustering algorithms and popular algorithm in the research of data mining field. It has the potential ability to fast superpixel generation. However, the DBSCAN is not suitable for pixel clustering in SAR images due to the speckle noise. In this article, we define a new adaptive pixel dissimilarity measure for the SAR image and then optimize the DBSCAN to achieve rapid local pixel clustering.

For one SAR image, we define two sets that are named as labeled set and candidate set. Then a top-left nonedge pixel is assigned to a label as the first seed and added into the labeled set. The reason is to avoid the local clustering around the SAR image edge. The SAR image pixels can be divided into three kinds, i.e., the seed, labeled, and unlabeled pixels.

For the seed pixel, we find its four neighbor pixels that are unlabeled, then calculate the dissimilarity measures between the neighbor pixel and the seed pixel. If the dissimilarity is less than the threshold we defined, we give the neighbor pixels the same label as the seed and update the labeled set. We then find all of the unlabeled four neighbor pixels of each pixel in the newly updated labeled set, then calculate the dissimilarity measures between each unlabeled pixel and the seed. If the dissimilarity is less than the threshold, the unlabeled pixels will be labeled as the seed and the labeled set is updated. Note that this procedure is iterated until the termination condition is satisfied.

Afterward, the labeled set will be replaced by a candidate set and a new seed is selected with a conventional order from the unlabeled and nonedge pixels. The above procedure is repeated until all the pixels are labeled. Finally, initial superpixels are generated after getting enough candidate sets with different labels. Fig. 3 gives the illustration of the proposed pixel clustering, where Fig. 3(a) illustrates the unlabeled neighbor pixels of the seed pixel. The thick and thin edges between the seed and neighbor pixels denote the large and small dissimilarities. Fig. 3(b) gives the generation stage of the labeled set, i.e., the calculation of the dissimilarity between unlabeled four neighbor pixels of

Algorithm 1: The Edge Detector For SAR Images With Recurrent Guidance Filter.

Input: SAR image, number of iterations itr, edge extraction thresholds Th_{low} and Th_{high}.
Output: Edge strength map and edge pixels.
1: **for** each iteration in itr **do**
2: The given SAR image is filtered by the recurrent guidance filter with (2).
3: **end for**
4: In the filtered SAR image, **for** every pixel, **do**
5: the edge strength map can be calculated using the Gaussian-shaped edge detector.
6: **end for**
7: Perform the non-maximum suppression (NMS) on the edge strength map to get the maximum values which form the candidate edge pixels.
8: **for** every pixel in the candidate pixels **do**
9: **if** edge strength is bigger than Th_{high} **then**
10: this pixel is declared as strong edge pixels.
11: **end if**
12: **end for**
13: **for** other candidate pixels **do**
14: **if** edge strength is between Th_{low} and Th_{high} **then**
15: this pixel can be labeled as edge pixels if there are strong edge pixels surrounding them in four neighborhoods.
16: **end if**
17: **end for**

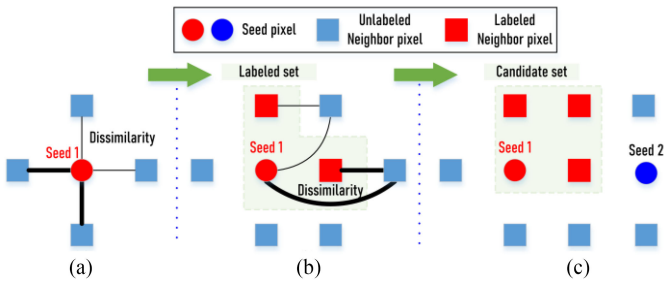

Fig. 3. Illustration of the fast clustering. (a) Unlabeled neighbor pixels of the seed pixel, where the thick and thin edges denote large and small dissimilarities. (b) Calculation of the dissimilarity between unlabeled four neighbor pixels of the labeled set and the seed. (c) Labeled set is replaced by the candidate set once the termination condition is satisfied.

the labeled set and the seed. The unlabeled neighbor pixels will change to labeled pixels once the dissimilarity measure is less than the defined threshold. Fig. 3(c) shows the candidate set result when the termination condition is satisfied, i.e., the size of labeled set reaches to the predefined superpixel size. The candidate set is regarded as the initial superpixel. Then the next seed is selected to generate a new candidate set.

The dissimilarity measure between the unlabeled pixel and seed plays a key role in superpixel generation. In this article, we propose a new adaptive pixel dissimilarity measure considering the edge penalty and SAR image homogeneity. The intensity dissimilarity $\delta(i,j)$ of pixels i and j can be defined based on the likelihood ratio test statistic using two patches Pi and Pj which are centering the two pixels as

$$\delta(i,j) = 2M \cdot L \cdot \ln \frac{\bar{I}_{Pi} + \bar{I}_{Pj}}{2\sqrt{\bar{I}_{Pi} \cdot \bar{I}_{Pj}}} \tag{5}$$

where $\bar{I}_{Pi}$ and $\bar{I}_{Pj}$ denote the average intensity of two patches. M is the number of pixels in the patch, which is usually set as 5×5. L is the number of looks of the SAR images. Aside from the intensity dissimilarity, pixels around the edges cannot be easily clustered. Therefore, we incorporate an edge penalty into the pixel dissimilarity as

$$\sigma(i,j) = \delta(i,j) + \frac{1}{2}[\xi(i) + \xi(j)] \tag{6}$$

where $\sigma(i,j)$ denotes the pixel dissimilarity between i and j. $\xi(i)$ and $\xi(j)$ are the edge strength of two pixels, which can be obtained by the edge detector [29]. In this way, pixels with larger edge strength will have larger dissimilarity, which avoids the clustering. In addition, due to the seed selection procedure, i.e., nonedge pixel, the edge penalty between seeds, and other pixels will be always effective. It is worth pointing out that for each unlabeled pixel, whether it should be clustered by the seed not only depends on the dissimilarity between them but also depends on the dissimilarity between the pixel and its center pixel for the reason that the unlabeled pixel is a neighbor of the center and the center is already clustered by the seed. As shown in Fig. 3(b), whether the rightmost unlabeled pixel can be clustered by the seed not only depends on the dissimilarity between the unlabeled pixel and the seed but also depends on the dissimilarity between the unlabeled pixel and its center pixel, which is the labeled neighbor pixel. Therefore, according to Fig. 3(b), we rewrite the dissimilarity between the unlabeled pixel j and the seed i as

$$\Omega(i,j) = \sigma(i,j) + |\mathcal{H}(i) - \mathcal{H}(j)| \cdot \sigma(k,j) \tag{7}$$

where $\Omega(i,j)$ denotes the adaptive dissimilarity measure. $\sigma(k,j)$ is the pixel dissimilarity between the center pixel k and the unlabeled pixel j. $\mathcal{H}(i)$ and $\mathcal{H}(j)$ represent the homogeneity of two pixels, which can be calculated by the coefficient of variation of SAR image as

$$\mathcal{H}(i) = \frac{\sigma_M(i)}{\bar{I}_M(i)} \tag{8}$$

where $\sigma_M(i)$ and $\bar{I}_M(i)$ denote the standard deviation and mean intensity of the local image region surrounding the pixel i, respectively. It can be found that in (7), if the unlabeled pixel locates in the heterogeneous areas, the homogeneity values of different pixels are quite different, thus $|\mathcal{H}(i) - \mathcal{H}(j)|$ will be large and $\sigma(k,j)$ plays a key role in $\Omega(i,j)$, resulting in that pixels having high similarity with k are more likely clustered by the seed. Therefore, the generated superpixels can well adhere to image boundaries and preserve image details. In contrast, if the unlabeled pixel locates in the homogeneous areas, $\Omega(i,j)$ will be dominated by the $\sigma(i,j)$. Thus, pixels that are similar to the seed will be clustered, making the superpixel regular.

In terms of the terminate condition, the superpixel size no more than the threshold S/K is selected, where S represents the SAR image size and K denotes the number of superpixels to be set. It can be seen that this condition is used to control the size of initial superpixels. It is worth pointing out that

the superpixel number K is the parameter that needs to be set for the proposed algorithm. More superpixels can generate more accurate segments, which can adhere well to the image boundaries. However, more superpixels will lead to a relatively high computation load for the following SAR data applications. Therefore, the superpixel number K should be determined depending on the SAR image size and the scene homogeneity. Although the proposed clustering procedure seems like region growing, the seed selection strategy and the terminate condition make the clustering fast and different from the slow region growing. Another issue that should be discussed is the dissimilarity threshold. Generally, two pixels are regarded as similar if their pixel intensities are 80% similar and the homogeneity values are almost the same. Note that it is an experience value and can be accepted in real applications. Moreover, the edge strength values of these two pixels are almost zero. Therefore, in this article, we can derive the dissimilarity threshold according to (7). When the homogeneity values are the same and the edge strength values are zero, the dissimilarity $\Omega(i,j)$ between the unlabeled pixel j and the seed i will be only determined by the $\delta(i,j)$. If we assume that two pixels are regarded as similar if their pixel intensities are 80% similar, then according to (5), the $\delta(i,j)$ can be calculated as

$$\begin{aligned}\delta(i,j) &= 2\cdot 25\cdot L\cdot \ln\frac{\bar{I}_{Pi}+0.8\cdot\bar{I}_{Pi}}{2\sqrt{\bar{I}_{Pi}\cdot 0.8\cdot\bar{I}_{Pi}}}\\ &= 50\cdot L\cdot\ln\frac{1.8}{2\sqrt{0.8}} = 0.31\cdot L. \end{aligned}\tag{9}$$

Therefore, the dissimilarity threshold in this article can be derived as $0.31\cdot L$ to determine the clustering.

C. Merging Stage Between Initial Superpixels

After the fast clustering, the merging stage here is used to merge the superpixels and eliminate small fragments, leading to final superpixel results. If the number of pixels within one initial superpixel is less than a threshold, we will merge it with its neighbor initial superpixel which has the lowest dissimilarity. After the merging stage, the final refined superpixels with the regular shapes can be obtained. Here we propose a new superpixel dissimilarity as

$$\begin{aligned}\Omega\left(SP_m,SP_n\right) &= \sigma\left(SP_m,SP_n\right)\\ &\quad+\frac{1}{2}\left(\xi\left(SP_m\right)+\xi\left(SP_n\right)\right)\\ &\quad+\left|\mathcal{H}\left(SP_m\right)-\mathcal{H}\left(SP_n\right)\right| \end{aligned}\tag{10}$$

$$\begin{aligned}\sigma\left(SP_m,SP_n\right) &= 2\cdot\min\left(\text{size}\left(SP_m\right),\text{size}\left(SP_n\right)\right)\\ &\quad\cdot L\cdot\ln\frac{\bar{I}_{SP_m}+\bar{I}_{SP_n}}{2\sqrt{\bar{I}_{SP_m}\cdot\bar{I}_{SP_n}}}\end{aligned}\tag{11}$$

where size $(\cdot)$ denotes the superpixel size. It can be seen from (10) that this superpixel dissimilarity considers intensity, edge, and homogeneity information. Thus, if two superpixels have similar intensity values and low edge response, as well as similar homogeneity will be easily merged. Regarding the superpixel size threshold, it can be set as $0.2\times(S/K)$, which is quite small in comparison with the initial superpixel size.

The detailed implementation of the proposed superpixel generation algorithm is given in Algorithm 2.

Algorithm 2: Superpixel Generation Based On Fast DBSCAN Clustering With Edge Penalty.

Input: SAR image with size S and number of looks L, the number of superpixels K.
Output: Superpixel generation result.
Edge extraction stage:
1: Perform edge extraction from the SAR image using the Algorithm 1.
Initialization stage:
2: The expected superpixel size is S/K. Calculate the homogeneity of each pixel, which can be obtained by the coefficient of variation of SAR image. Set initial pixel label as 0. Set the label set L_{set} and candidate set C_{set} empty.
Initial superpixel generation stage:
3: **while** find a seed i, optimize the seed with the edge strength, set $i\in L_{\text{set}}$, **do**
4: **while** the superpixel size is not larger than S/K, **do**
5: **for** each pixel j in L_{set}
6: **for** each pixel k neighboring to j
7: compute the adaptive dissimilarity measure $\Omega(i,j)$ for the seed i and pixel k.
8: **if** $\Omega(i,j)<0.31\cdot L$ **then**
9: set $k\in L_{\text{set}}$;
10: **end if**
11: **end for**
12: **end for**
13: set $C_{\text{set}}=L_{\text{set}}$;
14: **end while**
15: **end while**
Superpixel merging stage:
16: For each superpixel SP_m, **if** its superpixel size is less than $0.2\times(S/K)$, **then**
17: **for** each superpixel SP_n which is neighboring to SP_m, **do**
18: compute the superpixel dissimilarity $\Omega(SP_m,SP_n)$ between SP_m and SP_n;
19: find the smallest $\Omega(SP_m,SP_n)$ among the neighbor superpixels of SP_m;
20: set the label of SP_n as the label of SP_m;
21: merge the two superpixels.
22: **end for**
23: **end if**

IV. Experimental Results and Analysis

In this section, we demonstrate the performance of our method using two simulated and two real SAR datasets. Five representative methods, including the SLIC-PSR [12], the EA superpixel generation [11], the ED local clustering [13], the FV-based

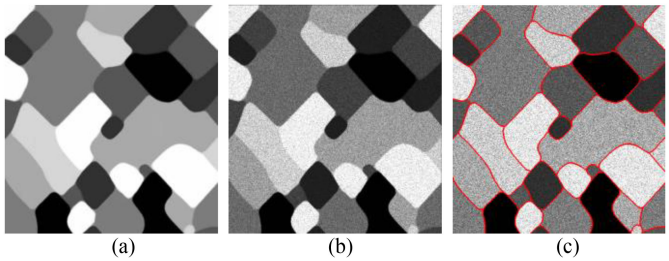

Fig. 4. First simulated SAR image with Gamma speckle and the corresponding ground truth. (a) Texture image. (b) Simulated SAR image with four-look Gamma speckle. (c) Ground truth map.

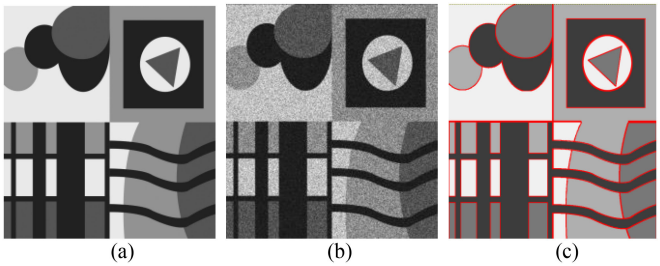

Fig. 5. Second simulated SAR image with Gamma speckle and the corresponding ground truth. (a) Texture image. (b) Simulated SAR image with two-look Gamma speckle. (c) Ground truth map.

adaptive superpixel segmentation (FVASS) [16], and the superpixel segmentation method of superpixel boundary-based edge description algorithm (Sp-SpBED) [17] are selected for comparison. Note that the EA and ED methods both consider the edge information for superpixel generation but without considering the SAR image homogeneity. The edges are regarded as constraints or guidance information for the following local clustering. PSR is a generally superpixel method based on the SLIC without considering the edge and homogeneity information. FVASS is a superpixel generation method designed for SAR marine images, which is further demonstrated by using ship detection. The Sp-SpBED method calculates the neighborhood weighted mean of each superpixel to achieve the final superpixel smoothing, which can obtain accurate superpixels. Note that the edge strength maps for EA, ED, and our method are all the same, leading to a fair comparison on the superpixel generation. For all the comparison methods, we select the optimal parameters according to the corresponding references, which can achieve the optimal superpixel segmentation results.

A. *Superpixel Results of the Simulated SAR Dataset*

Figs. 4 and 5 give the simulated SAR images and the corresponding ground truth. Figs. 4(a) and 5(a) display the original simulated texture images, where the image sizes are 512×479 and 800×800, respectively. It should be noted that the texture images have clear boundaries, which would be beneficial to analyze and evaluate the superpixel segmentation performance. Figs. 4(b) and 5(b) show the simulated SAR image with four-look and two-look Gamma speckle, respectively. In the simulation, we generate four-look and two-look Gamma speckle-noise

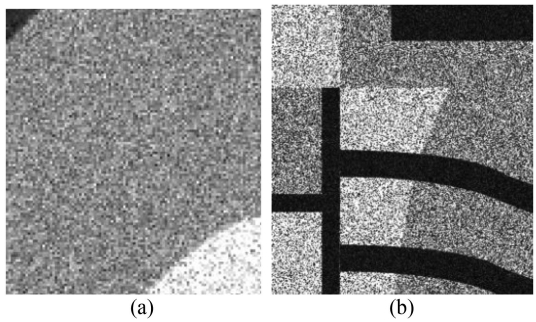

Fig. 6. Selected patch from the simulated SAR images. (a) Homogeneous area from the first simulated SAR image with four-look Gamma speckle. (b) Heterogeneous area from the second simulated SAR image with two-look Gamma speckle.

images and then multiply them with the texture images to obtain the final simulated SAR images. Note that the speckle is more serious with a lower number of looks of the Gamma speckle, as shown in Fig. 6. It can be seen that the second simulated SAR image has more serious multiplicative speckle noise than the first simulated one. Figs. 4(c) and 5(c) illustrate the ground truth maps of the corresponding SAR images, which are obtained manually by several experts.

Fig. 7 gives the superpixel generation results of six methods for the first simulated SAR image with four-look Gamma speckle, where the red boundary in the right part represents the superpixel map, and the left part indicates the average segmentation image. It can be found that in Fig. 7(a), the SLIC-PSR method cannot well adhere to the SAR image boundaries. Moreover, the generated superpixels are not homogeneous. In contrast, the EA superpixel method and the ED local clustering method have better superpixel results with good boundary adherence due to the edge information assistance, as shown in Fig. 7(b) and (c). The method in Fig. 7(d) is designed based on the SLIC and FVs, which considers the SAR image statistics for the superpixel generation. Therefore, the result in Fig. 7(d) can consider the SAR image gradient information without the edge constraint thanks to the FV. The object boundaries can be well preserved and the segmentation accuracy is fine. However, this method is not robust to the speckle within the SAR image. The method in Fig. 7(e) is a SLIC method with image boundary assistance, which also shows good performance on SAR image superpixel generation. Nevertheless, the edges between different superpixels are not smooth due to the strong edge selection within the Sp-SpBED method. Therefore, there are some errors between the superpixels near the image boundaries. The result in Fig. 7(f) is quite satisfactory, where the superpixels can well adhere to image boundaries, moreover, the pixels within superpixels are more homogeneous than other methods, thanks to the homogeneity in the dissimilarity measure. In contrast, the other methods may generate irregular superpixels due to the speckle within the SAR image, leading to a large standard deviation for the homogeneous areas in the final segmentation result.

Fig. 8 shows the superpixel generation results of different methods for the second simulated SAR image with a two-look

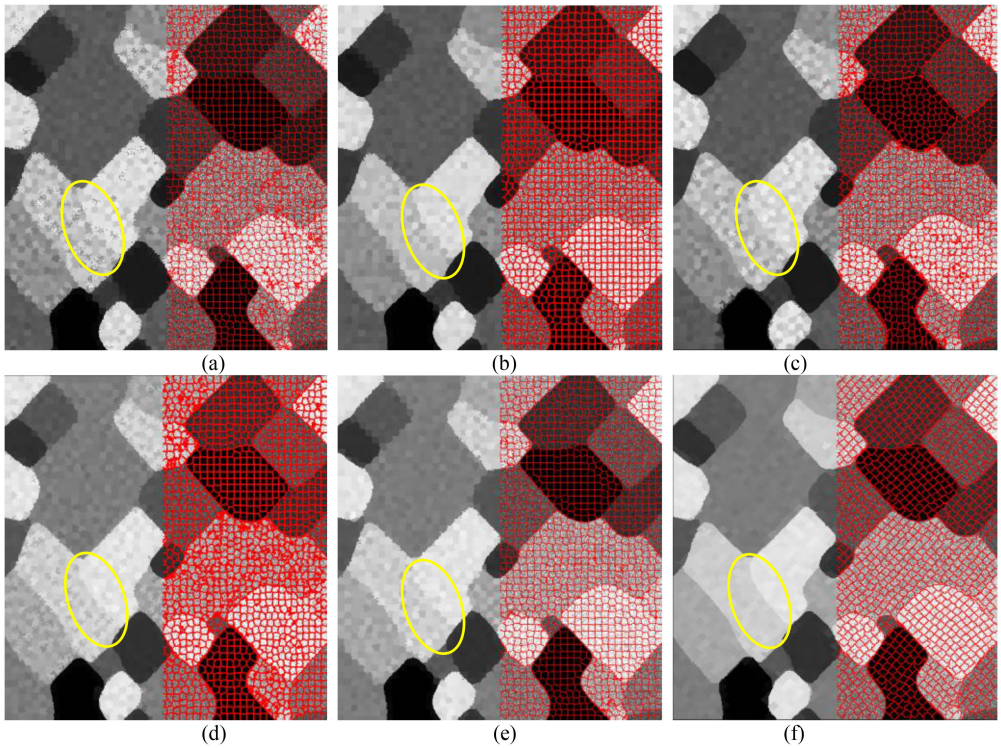

Fig. 7. Superpixel generation results of the first simulated SAR image with six methods. (a) PSR. (b) EA. (c) ED. (d) FVASS. (e) Sp-SpBED. (f) Our proposed method. The superpixel number is set to 2500 for all the results.

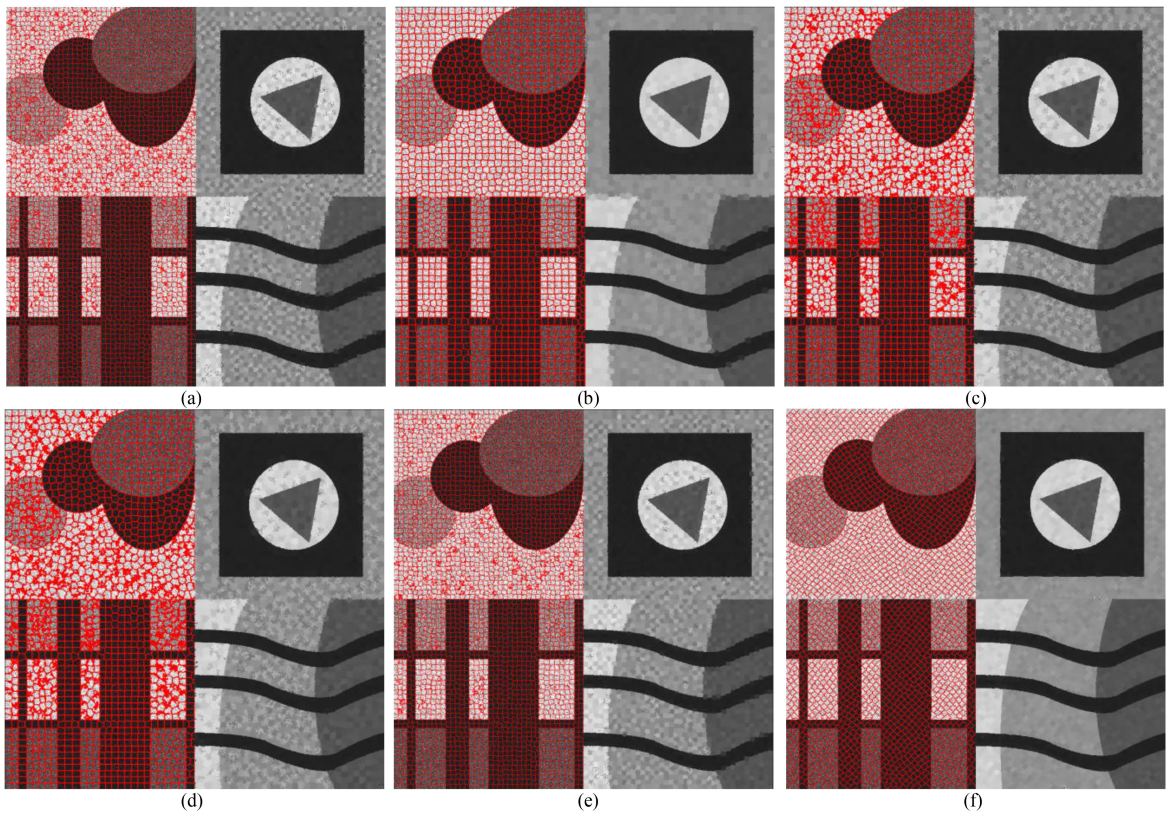

Fig. 8. Superpixel generation results of the second simulated SAR image with six methods. (a) PSR. (b) EA. (c) ED. (d) FVASS. (e) Sp-SpBED. (f) Our proposed method. The superpixel number is set to 3500 for all the results.

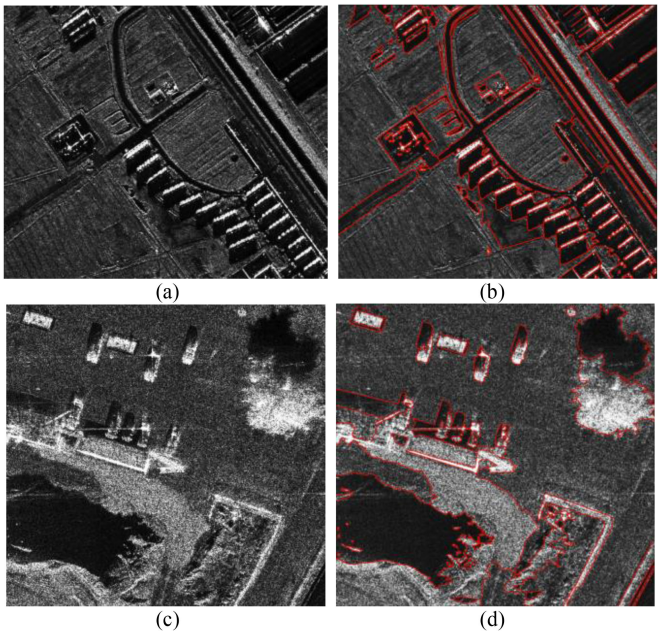

Fig. 9. Real SAR images and the corresponding ground truth. (a) and (c) CETC X band data and MiniSAR Ka band data, respectively. (b) and (d) Corresponding ground truth.

Gamma speckle. From this figure, it can be seen that with the increasing of speckle noise, most of the methods cannot well generate satisfactory superpixels for the simulated SAR image. For instance, in Fig. 8(a)–(e), there are many irregular superpixels within the homogeneous areas, indicating that the PSR, ED, FVASS, and Sp-SpBED methods cannot adaptively generate superpixels for the homogeneous and heterogeneous SAR scenes. Although the edges can be clearly preserved, the average segmentation results have relatively high standard deviations, degrading the superpixel segmentation accuracy. The result in Fig. 8(b) is fine for the reason that the edge information assists the superpixel generation. However, in contrast with the result in Fig. 8(f), the edge preservation is not so good. The proposed method can generate regular superpixels in the homogeneous SAR areas and can well adhere to the object boundaries due to the pixel dissimilarity and the superpixel dissimilarity, which take the edge penalty into consideration.

B. Superpixel Results of the Real SAR Datasets

Fig. 9 presents two real SAR images acquired by different sensors and the corresponding ground truth. Fig. 9(a) and (b) shows a four-look X band image from the CETC airborne SAR sensor of China and the ground truth, respectively. The image resolution is 0.5 m and the size is 587×690. Fig. 9(c) presents a single-look miniSAR Ka band airborne SAR image, which was acquired by the Sandia National Laboratories of USA and contains different land covers. The image size is 706×780 and the image resolution is 0.1 m. Fig. 9(d) shows its corresponding ground truth. It is worth pointing out that the ground truth images are obtained manually by several experts. Fig. 10 depicts the superpixel generation results of the CETC X band SAR image with different methods, where the number of superpixels is set to 4000 for all the results. It can be found in Fig. 10(a) that although the SLIC-PSR method can generate superpixels that can preserve the SAR image details to some extent, the superpixels cannot well adhere to the image boundaries, indicating that the SAR edge information is not fully utilized in the superpixel generation. Furthermore, the texture details cannot be well preserved, such as the yellow rectangular area. The results in Fig. 10(b) and (c) are better than that in Fig. 10(a) for the reason that the EA superpixel method and ED local clustering method both consider the edge information, which can make the generated superpixels well adhere to the image boundaries. It can be seen from Fig. 10(c) that the edges are well preserved in the superpixel map, leading to a better performance than that in Fig. 10(b). The results in Fig. 10(d) and (e) are similar to those in Fig. 10(a) since the FVASS and Sp-SpBED methods are also based on the SILC strategy. Specifically, since the FV features are considered in the superpixel generation, the segmentation performance is satisfactory for the man-made structures. However, the textural information within the homogeneous cannot be well preserved, such as the area marked with a yellow rectangle. The Sp-SpBED method has a similar performance with the FVASS approach, where the man-made structures are well preserved whereas the information in the homogeneous areas is missing in the superpixel segmentation result. The result in Fig. 10(f) is the best among different methods, thanks to the edge penalty and the homogeneity in the dissimilarity measure. The superpixels not only can adhere to image boundaries but also can preserve the textural details, such as the yellow rectangular area in Fig. 10(f). In contrast, the results of other methods are not satisfactory. For example, the roads in the SAR image can be well segmented with our method whereas are not well discriminated by other comparison methods.

Fig. 11 shows the superpixel generation results of the MiniSAR Ka band data with different methods and the superpixel number is set to 4000 for all the methods. What we can see from Fig. 11 that although the six methods can generate satisfactory superpixels for the Ka band SAR image, our proposed method can better preserve the image details and texture information than the other five methods, such as the yellow circular area in Fig. 11(f). Moreover, we can also observe that the superpixels of our method in homogeneous areas are quite regular and homogeneous, which are the same as Fig. 11(a) and (b). In contrast, the superpixels in Fig. 11(c) have irregular shapes to achieve good edge preservation. The results in Fig. 11(d) and (e) are slightly worse than other results due to the serious SAR speckle noise. For instance, in the natural homogeneous areas, the superpixels are quite irregular, indicating that the speckle noise has a great influence on the superpixel segmentation. In contrast, in the areas where the speckle is relatively weak, the segmentation performance is fine. The reason is that the selected features in the FVASS and Sp-SpBED methods cannot handle the serious speckle within SAR images. The satisfactory result in Fig. 11(f) indicates that the proposed

method considers the edge penalty and the homogeneity in the fast clustering and superpixel merging. Therefore, the superpixels can be adaptively generated in homogeneous and

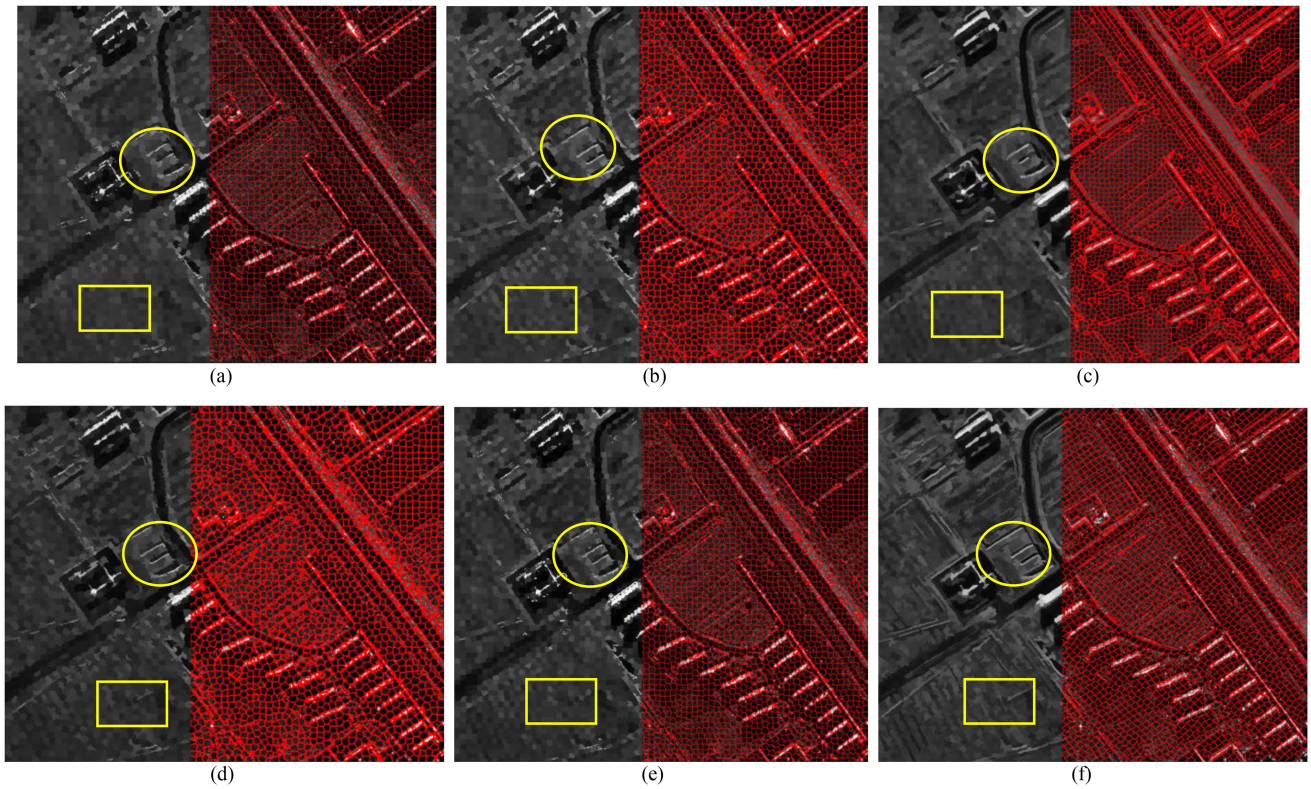

Fig. 10. Superpixel generation results of the CETC X band image with different methods. (a) PSR. (b) EA. (c) ED. (d) FVASS. (e) Sp-SpBED. (f) Our proposed method. The superpixel number is set to 4000 for all the results.

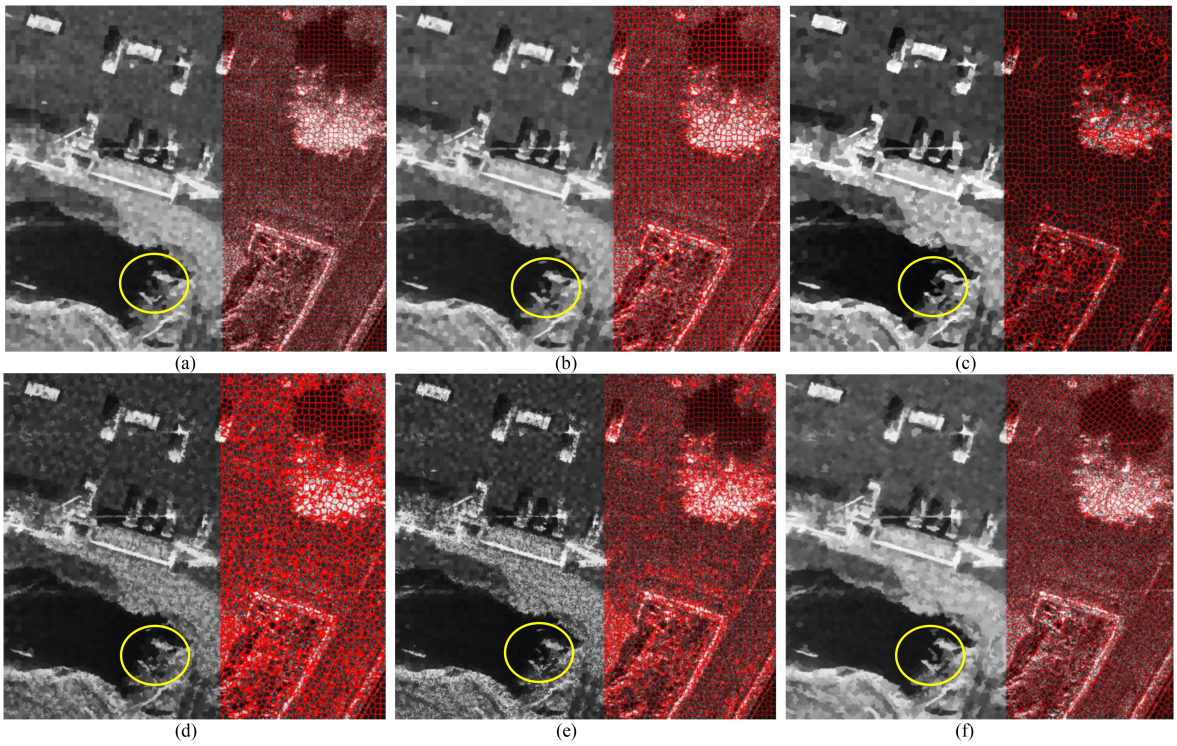

Fig. 11. Superpixel generation results of the MiniSAR Ka band image with different methods. (a) PSR. (b) EA. (c) ED. (d) FVASS. (e) Sp-SpBED. (f) Our proposed method. The superpixel number is set to 4000 for all the results.

heterogeneous areas with good boundaries adherence. Moreover, the detailed information can be well preserved, which is beneficial to the post applications of SAR data.

C. Quantitative Comparison of Different Methods

To further quantitatively evaluate the performance of different methods, the boundary recall (BR) [8] and the under-segmentation error (UE) [8] are chosen as the standard metrics. The BR is defined as the percentage of ground truth boundaries recovered by the superpixel edges [16]. It should be noted that higher BR values denote better boundary adherence for the generated superpixels. The formula definition of the BR is depicted as

$$BR = \frac{1}{\left|\mathcal{B}^{(g)}\right|} \sum_{b \in \mathcal{B}^{(g)}} 1 \left[\left(\min_{a \in \mathcal{B}^{(s)}} \sqrt{(x_a - x_b)^2 + (y_a - y_b)^2} \right) \leqslant \varepsilon \right] \quad (12)$$

where $\mathcal{B}^{(g)}$ and $\mathcal{B}^{(s)}$ denote the boundary pixels in the ground truth result and the generated superpixel segmentation result, respectively. The operator $1[\cdot]$ is 1 if the input parameter is true and 0 if the input parameter is false. The symbol $|\cdot|$ indicates the number of elements in an input set. (x_a, y_a) and (x_b, y_b) are the pixel coordinates of the boundary pixels in the set $\mathcal{B}^{(s)}$ and $\mathcal{B}^{(g)}$, respectively. The parameter ε represents the boundary tolerance factor, which is generally set to 3 [16]. The UE is another measure of boundary adherence, which evaluates the conciseness of the generated superpixels. Let s_l and g_z be the lth generated superpixel and zth ground truth segment in the SAR image, respectively. Then the UE is expressed as

$$\mathrm{UE} = \frac{1}{|I|} \left[\sum_{i=1}^{\left|\mathcal{B}^{(g)}\right|} \left(\sum_{s_j | s_j \cap g_i > \vartheta(s_j)} |s_j| \right) - |I| \right] \quad (13)$$

where $|I|$ denotes the number of pixels in SAR image I. $s_j | s_j \cap g_i$ means how many pixels from s_j covered by the boundary pixels of g_i. The parameter $\vartheta(s_j)$ indicates the tolerance factor, which is set to 3 percent of $|s_j|$ in our experiments to account for ambiguities in the ground truth. It is worth pointing out that superpixels that do not well fit the ground truth lead to a high value of UE. Therefore, lower UE values represent better superpixel segmentation results.

In order to demonstrate the robustness of different methods to the multiplicative speckle, we quantitatively evaluate the superpixel generation results of different methods for the two simulated SAR images with different number of looks Gamma speckle. The BR and UE curves are shown in Fig. 12, where the first row of Fig. 12 depicts the BR and UE results of the first simulated SAR image with four-look Gamma speckle. The second row of Fig. 12 denotes the BR and UE results of the second simulated SAR image with two-look Gamma speckle, which has more serious speckle in comparison with the four-look Gamma speckle. The superpixel number is changed from 1000 to 3000 with step 500 for all the results. It can be seen that although the speckle of SAR image increases, our method still has relatively high *BR* values and low *UE* values, demonstrating the robustness of the proposed method to the speckle noise. Although there exists a light decrease of the BR value and increase of the UE value for our method when the speckle becomes more serious, the superpixel segmentation performance is still satisfactory with BR above 0.9 and UE below 0.4 when the superpixel number exceeds 2000. In contrast, the BR values of the other five methods are lower, especially the PSR, FVASS, and Sp-SpBED methods when the superpixel number is less than 2000.

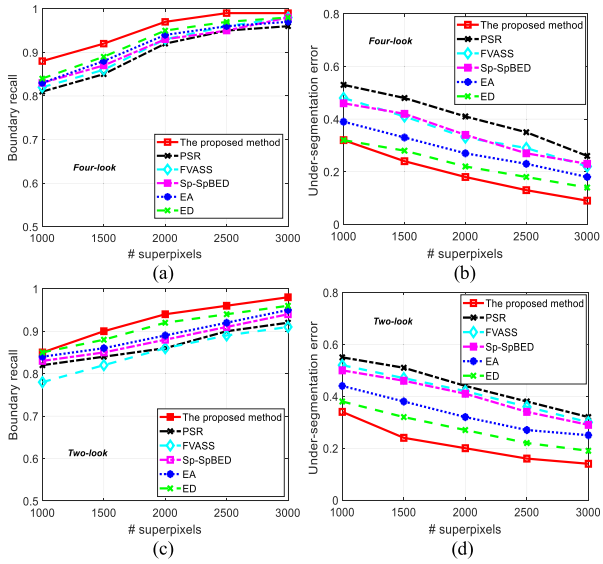

Fig. 12. BR and UE curves with different superpixel numbers of different methods for the two simulated SAR images. The first row denotes the BR (a) and UE (b) results of the first simulated SAR image with four-look Gamma speckle. The second row denotes the BR (c) and UE (d) results of the second simulated SAR image with two-look Gamma speckle.

In order to further evaluate the superpixel generation performance of different methods with regard to various levels of speckle noise, the simulated SAR images with one-look and six-look Gamma speckle are utilized to compute the BR and UE values of different methods. The number of superpixels is set to 2000. Table I gives the BR and UE values of different methods for the two simulated SAR images with one-look and six-look gamma speckle, respectively. From this table, it can be found that our proposed method has a much stronger ability against the SAR image speckle in comparison with other methods. The BR values of our proposed superpixel generation method are all above 0.9 even for the SAR images with serious one-look Gamma speckle, indicating that the proposed method is robust to SAR image speckle. In contrast, the BR values of other methods change accordingly with the different levels of speckle, indicating that these methods would be influenced by the speckle. Moreover, the UE values of our proposed method are much lower than other methods for different SAR images, which benefit from the edge information and homogeneity contained in the pixel and superpixel dissimilarity of our method.

Fig. 13 gives the quantitative evaluation measures of different methods for the two real SAR images, where the first row denotes the BR and UE curves for the CETC X band SAR image and

TABLE I
BR AND UE VALUES OF DIFFERENT METHODS FOR THE TWO SIMULATED SAR IMAGES WITH ONE-LOOK AND SIX-LOOK GAMMA SPECKLE

Methods	Level of speckle	The proposed method		PSR		EA		ED		FVASS		Sp-SpBED	
		BR	*UE*	*BR*	*UE*	*BR*	*UE*	*BR*	*UE*	*BR*	*UE*	*BR*	*UE*
The first simulated SAR image	One-look	0.93	0.22	0.82	0.49	0.86	0.34	0.88	0.29	0.82	0.46	0.83	0.44
	Six-look	0.95	0.20	0.86	0.41	0.89	0.29	0.89	0.25	0.87	0.41	0.89	0.39
The second simulated SAR image	One-look	0.92	0.25	0.81	0.48	0.85	0.37	0.87	0.31	0.81	0.47	0.82	0.45
	Six-look	0.93	0.22	0.84	0.42	0.87	0.31	0.89	0.28	0.85	0.44	0.86	0.41

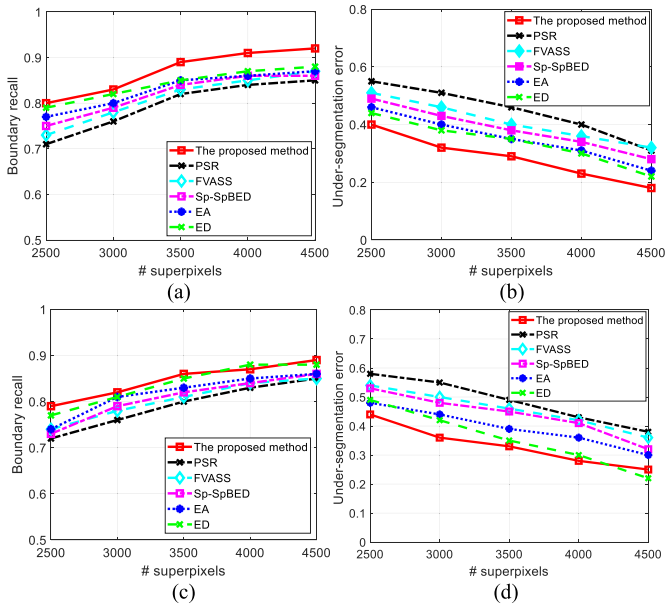

Fig. 13. BR and UE curves with different superpixel numbers of different methods for the two real SAR images. The first row denotes the (a) BR and (b) UE results of the CETC X band SAR image. The second row denotes the (c) BR and (d) UE results of the MiniSAR Ka band SAR image.

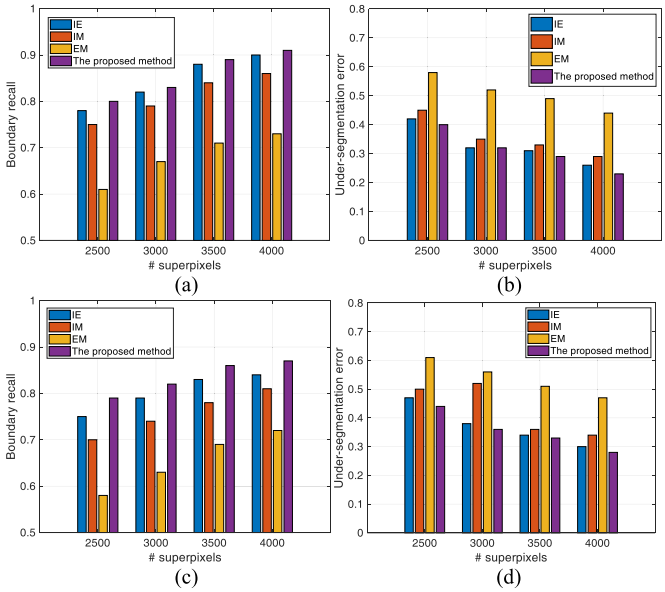

Fig. 14. BR and UE values of our method with different components under different superpixel numbers for the two real SAR images. The first row denotes the BR (a) and UE (b) results of the CETC X band SAR image. The second row denotes the BR (c) and UE (d) results of the MiniSAR Ka band SAR image.

the second row shows the BR and UE results for the MiniSAR Ka band SAR image. The superpixel number is changed from 2500 to 4500 with step 500 for all the results. From Fig. 13 we can observe that our proposed method has higher BR values and lower UE values in comparison with other state-of-the-art methods, indicating that for real SAR images, the generated superpixels not only can well adhere to the image boundaries but also can obtain accurate segments with homogeneous inside pixels. Therefore, the superpixel segmentation results are beneficial to the further SAR image applications, such as the image classification task, which will be conducted and analyzed in Section IV-F.

D. In-Depth Analysis for the Individual Components of the Proposed Method

Note that the pixel dissimilarity measure in our proposed method plays a key role in the superpixel segmentation, we should pay more attention to the individual contributions of different parts of the dissimilarity measure, i.e., the intensity dissimilarity, edge penalty, and homogeneity measure. In Section III-B, we give the expressions for each component of the pixel dissimilarity and discuss the corresponding contributions. In this section, we further analyze the superpixel generation performance of different parts using the quantitative evaluation measures.

To illustrate the individual contribution of three parts of the pixel dissimilarity, we design three compared pixel dissimilarity measures which are intensity dissimilarity & edge penalty (namely *IE*), intensity dissimilarity & homogeneity measure (namely *IM*), and edge penalty & homogeneity measure (namely *EM*). Then we replace the proposed pixel dissimilarity measure in our method with the above three pixel dissimilarities to obtain three variants of our method for comparison. In order to discuss the superpixel generation performance with different superpixel number for the two real SAR images, the numbers 2500, 3000, 3500, 4000 are chosen for comparison.

Fig. 14 gives the BR and UE values of our method with different components under different superpixel numbers for the two real SAR images. The first row of Fig. 14 shows the BR and UE results of the CETC X band SAR image while the second row denotes the results of the MiniSAR Ka band SAR image. From Fig. 14(a) and (c), it can be found that without the homogeneity measure in the pixel dissimilarity, the superpixel segmentation

TABLE II
TIME COSTS OF DIFFERENT METHODS (SECONDS)

Methods	Datasets	Number of segments	
		2500	3000
The proposed method	X band	3.1	3.2
	Ka band	4.8	5.1
PSR	X band	3.7	3.9
	Ka band	4.8	5.0
EA	X band	6.5	6.6
	Ka band	7.8	7.9
ED	X band	7.2	7.4
	Ka band	11.1	11.3
FVASS	X band	13.2	13.6
	Ka band	15.7	16.4
Sp-SpBED	X band	6.2	6.4
	Ka band	7.5	7.6

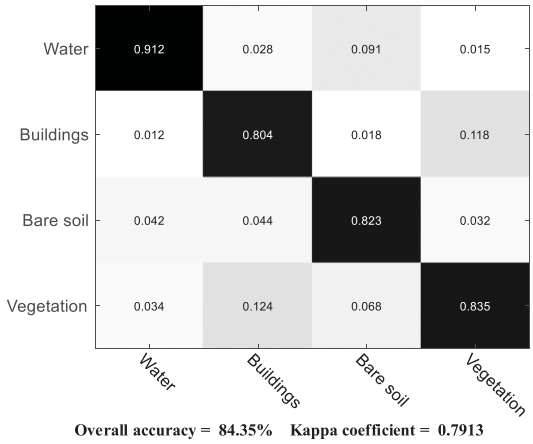

Fig. 15. Confusion matrix map of the classification result with the pixel-based K-Means classifier.

performance of our method has a slight decrease. In contrast, there exists a large decrease when the pixel dissimilarity only considers the edge penalty and homogeneity measure, indicating that the intensity dissimilarity plays a key role in the final pixel dissimilarity

for superpixel segmentation. When the edge penalty is omitted, the BR values of generated superpixels are much smaller in comparison with the originally proposed method. Therefore, it can be concluded that the edge penalty is quite essential to the superpixel generation, especially in terms of the image object boundary adherence.

Fig. 14(b) and (d) shows the UE results of two real SAR images, which reflect the region segmentation performance of the superpixels. From these two subfigures, we can observe that among the three components of the pixel dissimilarity, intensity dissimilarity is the most important factor in superpixel segmentation. Both the edge penalty and homogeneity measure contribute to the superpixel generation, especially the edge penalty, making the superpixels well adhere to the image boundaries and can obtain accurate segments for SAR images.

E. Computational Complexity Analysis

Considering that the proposed method mainly focuses on the fast clustering and merging for superpixel generation, here we only discuss the computational complexity of these two stages. The complexity of our proposed superpixel generation method is $O(K)$ for the reason that there does not exist any iteration process. Unlike the SLIC-based superpixel generation methods [12], [13] and the mixture-based method [11], the computational complexity of our proposed method only depends on the superpixel number, which is faster than most of the state-of-the-art superpixel algorithms.

The time costs of different methods for the two real SAR datasets are given in Table II. All the methods are implemented with MATLAB on a PC with 3.8 GHz i7 CPU. It is worth pointing out that the time costs are the total time spent by all methods. From this table, we can find that the proposed method can achieve fast superpixel generation even though with the consideration of edge extraction stage, which benefits from the fast clustering and merging strategy. In contrast, the EA superpixel and ED local clustering methods are slower, especially the latter method which performs iterative clustering for superpixel generation. The SLIC-PSR method also can quickly generate superpixels for the reason that there is no edge extraction stage in this method. However, the superpixel generation performance is not satisfactory. For the FVASS method, the computational complexity is relatively higher than other methods due to the feature analysis and computation. The Sp-SpBED method is similar to the PSR method, which is also designed on the basis of SLIC. Therefore, the computation is also efficient. From this table, it can be concluded that our proposed method can obtain satisfactory superpixel generation results for SAR images with relatively low computation cost in comparison with other state-of-the-art methods, which is quite beneficial to the post applications of SAR data.

F. Discussions on the SAR Image Applications Based on Superpixels

As stated in the previous sections, the generated superpixels are beneficial to the SAR image applications such as image classification and target detection, etc. To further demonstrate the advantages of superpixels on the SAR image interpretation, in this section, we conducted unsupervised image classification for the SAR images with pixels and superpixels, respectively. The MiniSAR Ka band image is selected as the test data and K-Means classifier is adopted as the classification method. The SAR image is classified for four unknown clusters, which are recognized and then labeled using the reference Google Earth map. The four classes are identified as Water, Buildings, Bare soil, and Vegetation. For superpixel-based classification with different superpixel generation methods, the numbers of superpixels are all set to 4000. Fig. 15 shows the confusion matrix map of the pixel-based K-Means classifier for the MiniSAR image, where the rows represent classified results and the columns represent true classes. In order to analyze the classification accuracy, quantitative analysis is made through two parameters, namely overall accuracy and Kappa coefficient [20], which indicate

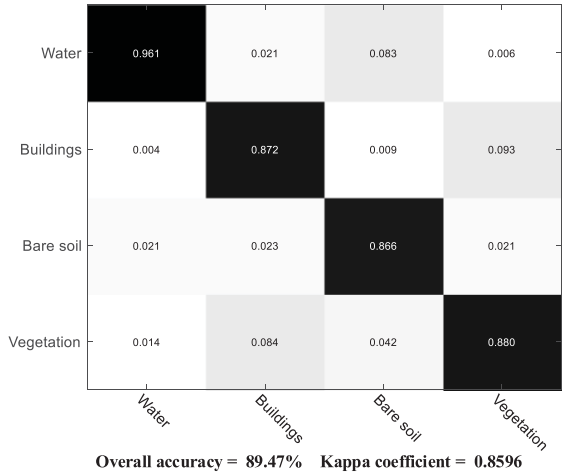

Fig. 16. Confusion matrix map of the superpixel-based classification with our proposed superpixel generation method

TABLE III
CLASSIFICATION ACCURACY OF THE SUPERPIXEL-BASED CLASSIFICATION WITH OTHER SUPERPIXEL GENERATION METHODS

	PSR	EA	ED	FVASS	Sp-SpBED
Overall accuracy	86.21%	88.18%	88.01%	87.26%	88.22%
Kappa coefficient	0.811	0.845	0.839	0.832	0.847

better classification results with higher values. Fig. 16 depicts the confusion matrix map of the superpixel-based K-Means classifier for the MiniSAR image, where the superpixels are regarded as processing units instead of pixels for classification. The superpixels are generated by our proposed method. Table III shows the five final overall classification accuracy results of other superpixel-based K-Means classifiers, where the superpixels are generated by using the PSR, EA, ED, FVASS, and Sp-SpBED, respectively.

From Figs. 15 and 16, we can find that with the assistance of superpixels, the confusion errors between forests and buildings are significantly reduced, leading to the improvement of classification accuracy. The reason is that the backscattering of buildings and forests in the Ka band SAR image is quite similar, which easily results in classification confusion with the pixel-based classifier. In contrast, the superpixel-based classifier can consider the neighborhood information around pixels, as well as the local geometrical information. Therefore, the classification accuracy can be improved. From Table III it can be seen that all the superpixel-based classification results have relatively higher accuracy and Kappa values than the pixel-based classification, demonstrating the advantages of superpixels in the SAR image classification task. It is also worth pointing out that the superpixel-based classification performance depends on the superpixel quality. Therefore, satisfactory superpixels with good boundary adherence and local homogeneity would achieve a fine image classification result.

The number of generated superpixels can also influence the classification performance, especially the efficiency. With the increase of superpixels, the image boundary can be well preserved. Nevertheless, there may be some over-segmentation errors, leading to classification confusion. More importantly, more superpixels would decrease the classification efficiency. Table IV gives the classification accuracy and efficiency of our proposed superpixel-based classification with a different number of superpixels. It can be found that when the superpixels increase from 2000 to 6000, the classification accuracy increases. However, when the superpixel number exceeds 6000, the overall accuracy does not have a large change. In contrast, the time costs are monotonically increasing with more superpixels. Therefore, it is not necessary that more superpixels would achieve better classification. Note that the selection of superpixel numbers in the classification depends on the complexity of the SAR image scene, as stated in the former sections in this article.

TABLE IV
CLASSIFICATION ACCURACY AND EFFICIENCY OF THE PROPOSED SUPERPIXEL-BASED CLASSIFICATION WITH DIFFERENT NUMBER OF SUPERPIXELS

	Number of superpixels				
	2000	4000	6000	8000	15000
Overall accuracy	86.15%	89.47%	90.15%	89.23%	89.36%
Time costs (s)	0.382	0.581	0.853	1.025	1.895

V. CONCLUSION

We propose an adaptive superpixel generation algorithm for SAR image in this article, which is implemented based on fast clustering and merging with edge penalty. An adaptive pixel dissimilarity measure and a superpixel dissimilarity measure are defined to achieve rapid clustering and small local superpixels merging, respectively. Experimental results demonstrate the priority of our proposed method, which can achieve fast and accurate superpixel generation for SAR images. Moreover, the unsupervised classification results also validate the advantages of superpixels, which can improve the classification accuracy, as well as the efficiency.

ACKNOWLEDGMENT

The authors would like to thank the Associate Editor and anonymous reviewers for their helpful suggestions, which greatly improved the quality of this article.

REFERENCES

[1] D. Hong, N. Yokoya, J. Chanussot, and X. X. Zhu, "An augmented linear mixing model to address spectral variability for hyperspectral unmixing," *IEEE Trans. Image Process.*, vol. 28, no. 4, pp. 1923–1938, Apr. 2018.
[2] T. Li, Z. Liu, L. Ran, and R. Xie, "Target detection by exploiting superpixel-level statistical dissimilarity for SAR imagery," *IEEE Geosci. Remote Sens. Lett.*, vol. 15, no. 4, pp. 562–566, Apr. 2018.
[3] O. Pappas, A. Achim, and D. Bull, "Superpixel-level CFAR detectors for ship detection in SAR imagery," *IEEE Geosci. Remote Sens. Lett.*, vol. 15, no. 9, pp. 1397–1401, Jun. 2018.
[4] R. Ghaffari *et al.*, "A fast, weighted CRF algorithm based on a two-step superpixel generation for SAR image segmentation," *Int. J. Remote Sens.*, vol. 41, no. 9, pp. 3535–3557, Jan. 2020.

[5] D. Xiang, T. Tang, L. Zhao, and Y. Su, "Superpixel generating algorithm based on pixel intensity and location similarity for SAR image classification," *IEEE Geosci. Remote Sens. Lett.*, vol. 10, no. 6, pp. 1414–1418, Nov. 2013.
[6] J. Shi and J. Malik, "Normalized cuts and image segmentation," *IEEE Trans. Pattern Anal. Mach. Intell.*, vol. 22, no. 8, pp. 888–905, Aug. 2000.
[7] A. Levinshtein, A. Stere, K. N. Kutulakos, D. J. Fleet, S. J. Dickinson, and K. Siddiqi, "Turbopixels: Fast superpixels using geometric flows," *IEEE Trans. Pattern Anal. Mach. Intell.*, vol. 31, no. 12, pp. 2290–2297, Dec. 2009.
[8] R. Achanta, A. Shaji, K. Smith, A. Lucchi, P. Fua, and S. Süsstrunk, "SLIC superpixels compared to state-of-the-art superpixel methods," *IEEE Trans. Pattern Anal. Mach. Intell.*, vol. 34, no. 11, pp. 2274–2282, Nov. 2012.
[9] J. Chen, Z. Li, and B. Huang, "Linear spectral clustering superpixel," *IEEE Trans. Image Process.*, vol. 26, no. 7, pp. 3317–3330, Jul. 2017.
[10] S. Arisoy and K. Kayabol, "Mixture-based superpixel segmentation and classification of SAR images," *IEEE Geosci. Remote Sens. Lett.*, vol. 13, no. 11, pp. 1721–1725, Nov. 2016.
[11] W. Jing, T. Jin, and D. Xiang, "Edge-aware superpixel generation for SAR imagery with one iteration merging," *IEEE Geosci. Remote Sens. Lett.*, vol. 18, no. 9, pp. 1600–1604, Sep. 2021.
[12] E. Akyilmaz and U. M. Leloglu, "Segmentation of SAR images using similarity ratios for generating and clustering superpixels," *Electron. Lett.*, vol. 52, no. 8, pp. 654–656, Apr. 2016.
[13] H. Hu *et al.*, "Superpixel generation for synthetic aperture radar imagery using edge-dominated local clustering," *J. Appl. Remote Sens.*, vol. 12, no. 4, 2018, Art. no. 045006.
[14] W. Zhang, D. Xiang, and Y. Su, "Fast multiscale superpixel segmentation for SAR imagery," *IEEE Geosci. Remote Sens. Lett.*, vol. 19, 2022, Art no. 4001805.
[15] R. Ghaffari *et al.*, "A fast, weighted CRF algorithm based on a two-step superpixel generation for SAR image segmentation," *Int. J. Remote Sens.*, vol. 41, no. 9, pp. 3535–3557, 2020.
[16] X. Wang, Y. He, G. Li, and A. Plaza, "Adaptive superpixel segmentation of marine SAR images by aggregating Fisher vectors," *IEEE J. Sel. Topics Appl. Earth Observ. Remote Sens.*, vol. 14, pp. 2058–2069, 2021.
[17] R. Shang, J. Lin, L. Jiao, X. Yang, and Y. Li, "Superpixel boundary-based edge description algorithm for SAR image segmentation," *IEEE J. Sel. Topics Appl. Earth Observ. Remote Sens.*, vol. 13, pp. 1972–1985, 2020.
[18] F. Yang, Q. Sun, H. Jin, and Z. Zhou, "Superpixel segmentation with fully convolutional networks," in *Proc. IEEE/CVF Conf. Comput. Vis. Pattern Recognit.*, 2020, pp. 13964–13973.
[19] N. Lv, C. Chen, T. Qiu, and A. K. Sangaiah, "Deep learning and superpixel feature extraction based on contractive autoencoder for change detection in SAR images," *IEEE Trans. Ind. Inf.*, vol. 14, no. 12, pp. 5530–5538, Dec. 2018.
[20] D. Hong *et al.*, "More diverse means better: Multimodal deep learning meets remote-sensing imagery classification," *IEEE Trans. Geosci. Remote Sens.*, vol. 59, no. 5, pp. 4340–4354, May 2020.
[21] D. Hong, L. Gao, J. Yao, B. Zhang, A. Plaza, and J. Chanussot, "Graph convolutional networks for hyperspectral image classification," *IEEE Trans. Geosci. Remote Sens.*, vol. 59, no. 7, pp. 5966–5978, Jul. 2021.
[22] S. Liu, Q. Shi, and L. Zhang, "Few-shot hyperspectral image classification with unknown classes using multitask deep learning," *IEEE Trans. Geosci. Remote Sens.*, vol. 59, no. 6, pp. 5085–5102, Jun. 2021.
[23] Q. Shi, M. Liu, S. Li, X. Liu, F. Wang, and L. Zhang, "A deeply supervised attention metric-based network and an open aerial image dataset for remote sensing change detection," *IEEE Trans. Geosci. Remote Sens.*, to be published, doi: 10.1109/TGRS.2021.3085870.
[24] Q. Shi, X. Tang, T. Yang, R. Liu, and L. Zhang, "Hyperspectral image denoising using a 3-D attention denoising network," *IEEE Trans. Geosci. Remote Sens.*, vol. 59, no. 12, pp. 10348–10363, Dec. 2021.
[25] J. Feng, Z. Cao, and Y. Pi, "Polarimetric contextual classification of PolSAR images using sparse representation and superpixels," *Remote Sens.*, vol. 6, no. 8, pp. 7158–7181, Jul. 2014.
[26] H. Song *et al.*, "Unsupervised classification of polarimetric SAR imagery using large-scale spectral clustering with spatial constraints," *Int. J. Remote Sens.*, vol. 36, no. 11, pp. 2816–2830, 2015.
[27] F. Lang *et al.*, "Superpixel segmentation of polarimetric synthetic aperture radar (sar) images based on generalized mean shift," *Remote Sens.*, vol. 10, no. 10, 2018, Art. no. 1592.
[28] J. Yin, T. Wang, Y. Du, X. Liu, L. Zhou, and J. Yang, "SLIC superpixel segmentation for polarimetric SAR images," *IEEE Trans. Geosci. Remote Sens.*, vol. 60, 2022, Art no. 5201317.
[29] W. Jing, T. Jin, and D. Xiang, "SAR image edge detection with recurrent guidance filter," *IEEE Geosci. Remote Sens. Lett.*, vol. 18, no. 6, pp. 1064–1068, Jun. 2021.
[30] D. Guan, D. Xiang, X. Tang, and G. Kuang, "SAR image despeckling based on nonlocal low-rank regularization," *IEEE Trans. Geosci. Remote Sens.*, vol. 57, no. 6, pp. 3472–3489, Jun. 2018.
[31] X. Yuan *et al.*, "Target recognition in SAR imagery based on local gradient ratio pattern," *Int. J. Remote Sens.*, vol. 35, no. 3, pp. 857–870, 2014.
[32] Y. Xiang *et al.*, "SAR-PC: Edge detection in SAR images via an advanced phase congruency model," *Remote Sens.*, vol. 9, Feb. 2017, Art. no. 209.
[33] Y. Xiang, F. Wang, L. Wan, and H. You, "An advanced multiscale edge detector based on Gabor filters for SAR imagery," *IEEE Geosci. Remote Sens. Lett.*, vol. 14, no. 9, pp. 1522–1526, Sep. 2017.
[34] P. Shui and D. Cheng, "Edge detector of SAR images using Gaussian-gamma-shaped Bi-windows," *IEEE Geosci. Remote Sens. Lett.*, vol. 9, no. 5, pp. 846–850, Sep. 2012.
[35] J. Shen, X. Hao, Z. Liang, Y. Liu, W. Wang, and L. Shao, "Real-time superpixel segmentation by DBSCAN clustering algorithm," *IEEE Trans. Image Process.*, vol. 25, no. 12, pp. 5933–5942, Oct. 2016.
[36] K. M. Kumar and A. R. M. Reddy, "A fast DBSCAN clustering algorithm by accelerating neighbor searching using groups method," *Pattern Recognit.*, vol. 58, pp. 39–48, Oct. 2016.

Liang Zhang received the B.S. and M.S. degrees in information and communication engineering from the National University of Defense Technology, Changsha, China, in 2005, 2007, respectively. He is currently working toward the Ph.D. degree in information and communication engineering with the College of Electronic Science, National University of Defense Technology.

His research interests include SAR image processing and machine learning.

Shengtao Lu received the B.S. degree in electronic science and technology from the Beijing University of Chemical Technology, Beijing, China, in 2020. He is currently working toward the M.S. degree in computer science and technology with the College of Information Science and Technology, Beijing University of Chemical Technology.

His research interests include machine learning and SAR image target detection.

Canbin Hu received the B.S., M.S., and Ph.D. degrees in information and communication engineering from the National University of Defense Technology, Changsha, China, in 2006, 2008, and 2014, respectively.

Since 2021, he has been a Lecturer with the College of Information Science and Technology, Beijing University of Chemical Technology, Beijing, China. His research interests include synthetic aperture radar (SAR)/polarimetric SAR image processing, and pattern recognition.

Deliang Xiang (Member, IEEE) received the B.S. degree in remote sensing science and technology from Wuhan University, Wuhan, China, in 2010, the M.S. degree in photogrammetry and remote sensing from the National University of Defense Technology, Changsha, China, in 2012, and the Ph.D. degree in geoinformatics from the KTH Royal Institute of Technology, Stockholm, Sweden, in 2016.

Since 2020, he has been a Full Professor with Interdisciplinary Research Center for Artificial Intelligence, the Beijing University of Chemical Technology, Beijing, China. His research interests include urban remote sensing, synthetic aperture radar (SAR)/polarimetric SAR image processing, artificial intelligence, and pattern recognition.

Dr. Xiang serves as a Reviewer for *Remote Sensing of Environment*, *ISPRS Journal of Photogrammetry and Remote Sensing*, IEEE TRANSACTIONS ON GEOSCIENCE AND REMOTE SENSING, IEEE JOURNAL OF SELECTED TOPICS IN APPLIED EARTH OBSERVATIONS AND REMOTE SENSING, IEEE GEOSCIENCE AND REMOTE SENSING LETTERS, and several other international journals in the remote sensing field. In 2019, he was the recipient of Humboldt Research Fellowship.

Tao Liu received the B.S. degree in electronic science and technology from Shanghai Jiaotong University, Shanghai, China, in 2011, the M.S. and Ph.D. degrees in information and communication engineering from the National University of Defense Technology, Changsha, China, in 2013, and 2018, respectively.

He is currently a Lecturer with the College of Electronic Science, National University of Defense Technology. His research interests include synthetic aperture radar signal processing.

Yi Su (Senior Member, IEEE) was born in Shandong, China, in 1961. He received the B.S., M.S., and Ph.D. degrees in electronic engineering from the School of Electrical Engineering, National University of Defense Technology, Changsha, China, in 1982, 1988, and 2001, respectively.

He has been a Professor with the School of Electronic Science Engineering, National University of Defense Technology. His research interests include signal processing, radar target characteristics, UWB radar, and remote sensing.